AAPS PharmSciTech (2024) 25:183
https://doi.org/10.1208/s12249-024-02902-x

RESEARCH ARTICLE

Preparation, Characterization and Evaluation of Nintedanib Amorphous Solid Dispersions with Enhanced Oral Bioavailability

Shuyin Liu[1,2] · Hui Chen[2] · Feng Zhou[2] · Sandip Tiwari[3] · Kai Zhuang[4] · Yudong Shan[5] · Jiantao Zhang[1,2]

Received: 21 March 2024 / Accepted: 26 July 2024 / Published online: 13 August 2024

Abstract

The dissolution and bioavailability challenges posed by poorly water-soluble drugs continue to drive innovation in pharmaceutical formulation design. Nintedanib (NDNB) is a typical BCS class II drug that has been utilized to treat idiopathic pulmonary fibrosis (IPF). Due to the low solubility, its oral bioavailability is relatively low, limiting its therapeutical effectiveness. It is crucial to enhance the dissolution and the oral bioavailability of NDNB. In this study, we focused on the preparation of amorphous solid dispersions (ASD) using hot melt extrusion (HME). The formulation employed Kollidon® VA64 (VA64) as the polymer matrix, blended with the NDNB at a ratio of 9:1. HME was conducted at temperatures ranging from 80 °C to 220 °C. The successful preparation of ASD was confirmed through various tests including polarized light microscopy (PLM), X-ray powder diffraction (XRPD), differential scanning calorimetry (DSC), Fourier-transform infrared spectroscopy (FT-IR), and thermogravimetric analysis (TGA). The *in-vitro* cumulative release of NDNB-ASD in 2 h in a pH 6.8 medium was 8.3-fold higher than that of NDNB ($p < 0.0001$). In a pH 7.4 medium, it was 10 times higher ($p < 0.0001$). In the *in-vivo* pharmacokinetic experiments, the area under curve (AUC) of NDNB-ASD was 5.3-fold higher than that of NDNB and 2.2 times higher than that of commercially available soft capsules (Ofev®) ($p < 0.0001$). There was no recrystallization after 6 months under accelarated storage test. Our study indicated that NDNB-ASD can enhance the absorption of NDNB, thus providing a promising method to improve NDNB bioavailability in oral dosages.

Keywords amorphous solid dispersion · hot melt extrusion · nintedanib · oral bioavailability

Introduction

Oral drug delivery is widely favored due to its convenience for drug administration, cost-effectiveness, non-invasiveness and high patient compliance [1]. Oral formulations hold approximately 90% of the global market share for all pharmaceutical formulations designed for human use. Among the top-selling pharmaceutical products, orally administered medications constitute around 84% [2, 3]. Although these dosage forms are popular, significant challenges remain. Drug oral absorption is influenced by many factors, such as drug solubility, mucosal permeability, and stability within the gastrointestinal environment. According to the biopharmaceutics classification system (BCS), a majority of oral drugs, especially many new entities, are categorized as BCS Class II or IV [4], meaning they exhibit either low solubility and high permeability, or low solubility and low permeability. Poorly water-soluble drugs often exhibit low bioavailability, limiting their therapeutic effectiveness [5]. For these drugs, achieving sufficient dissolution and permeability is the scientific issue that urgently needs to be addressed [6].

Nintedanib (NDNB) is a small molecule tyrosine kinase inhibitor, which was orally administered and approved by the US Food and Drug Administration (FDA) in October 2014 to treat idiopathic pulmonary fibrosis (IPF) [7]. It is

✉ Jiantao Zhang
Zhangjiantao@nimte.ac.cn

1 Cixi Biomedical Research Institute, Wenzhou Medical University, Cixi 315300, China

2 Laboratory of Advanced Theranostic Materials and Technology, Ningbo Institute of Materials Technology and Engineering, CAS, Ningbo 315201, China

3 Pharma Solutions, BASF Corp., 500 White Plains Rd, Tarrytown, NY 10591, USA

4 Pharma Solutions, Nutrition and Health, BASF (China) Company, Ltd, 333 Jiang Xin Sha Road, Shanghai 200137, China

5 Hangzhou Zhongmeihuadong Pharmaceutical Co., Ltd., 866 Moganshan Road, Hangzhou 310011, China

formulated in soft capsules, branded as Ofev® and Vargatef®, and is administered twice daily [8]. However, its oral bioavailability is limited, approximately only 4.7%, due to its extremely poor solubility [9–11]. Furthermore, studies have also identified issues related to the administration of higher doses of NDNB, including a higher incidence of side effects, such as diarrhea, gastrointestinal reactions, and liver impairment, and elevated costs as well [12–14].

To address this issue, various formulation strategies, including inclusion compounds [15], self-microemulsion [9], and solid dispersions [16], have been explored to enhance the solubility, dissolution rate, and ultimately bioavailability of NDNB. However, each method has its limitations. Inclusion compounds may result in delayed or uneven drug release in the body [17]. Self-microemulsion requires precise control during preparation, posing challenges to drug conversion and efficiency [18]. Solvent-based methods for solid dispersion may lead to solvent residue, potentially impacting drug stability and safety [19]. Therefore, there is a need to address the limitations of existing technologies by developing a more effective and convenient improved formulation to enhance the solubility of NDNB, thus improving its oral bioavailability.

One prominent approach to overcoming these challenges is the use of amorphous solid dispersions (ASDs) [20]. The active pharmaceutical ingredient (API) could be dissolved or dispersed within a suitable carrier or matrix in a solid state to form ASDs [21]. To obtain instant-release properties in ASDs, hydrophilic polymers are frequently used for their better wettability and solubilization capabilities [22]. These carriers can promote momentary supersaturation and provide a driving force to enhanced drug absorption [23]. ASD technology offers advantages of reduced particle size, improved wettability, and enhanced dissolution, thereby potentially improving drug absorption [24, 25]. Among the various techniques for preparing ASDs, hot-melt extrusion (HME) [26] stands out as a promising method, as it allows for solvent-free processing and is conducive to continuous industrial production.

The primary objective of this study is to develop NDNB amorphous solid dispersions (NDNB-ASDs) using VA64 as a solubilizing carrier material via HME technology, aiming for the simplest formulation possible. VA64 is a copolymer of vinylpyrrolidone and vinyl acetate and offers several advantages when used in HME drug formulations, including improved dissolution rate, enhanced mechanical properties, higher drug loading, and taste-masking effects [27, 28]. VA64 was selected for the formulation development due to the facts that it is an approved polymer listed in FDA IID list and has been used in development of many commercial ASD products. Additionally, it has a low glass temperature (101 °C), high temperature resistance and optimum rheological properties for HME. It also exhibits high solubilization capacity to many water-insoluble actives through forming ASD [29]. As shown in Figure S1, we conducted a preliminary screening of three different drug/polymer ratios (10%, 20%, and 30%) using a solvent evaporation method and based on the observation of drug recrystallization in the films, the 10% drug loading was found to be optimal for the ASD preparation through HME. Through process optimization, we found that the dissolution rate of NDNB formulated with VA64 in a 1:9 ratio was increased by 7.3-fold compared to the NDNB ($p < 0.0001$), leading to a 5.3-fold enhancement *in-vivo* absorption ($p < 0.0001$). Our study may provide valuable insights for the design and development of solid dispersion formulations using HME technology, paving the way for improved oral delivery of poorly soluble drugs to enhance therapeutic efficacy.

Material and Methods

Materials

Nintedanib (NDNB) was purchased from Shanghai Yuanye Biotechnology Co., Ltd. (Shanghai, China). The vinylpyrrolidone vinyl acetate copolymer (Kollidon® VA64, VA64) was kindly provided by BASF (Shanghai, China). Soft capsules (Ofev®) were purchased from Shiyao Group Enbipu Pharmaceutical Co., Ltd. (Shijiazhuang, China). Methanol (MeOH, HPLC-grade) was purchased from Macklin Industrial Co. (Shanghai, China). Triethylamine (AR, 99.0%) was purchased from Aladdin Biochemical Technology Co., Ltd. (Shanghai, China). Piperine (HPLC, ≥ 98%) was purchased from Macklin Industrial Co. (Shanghai, China).

Animals: 12 SPF-grade adult male SD rats, 10 to 12 weeks old, weighing 180 to 200 g, were maintained in a room (20–25 °C and 50–60% humidity) under a 12 light/dark cycle, with free access to standard rodent chow and clean water for 7 days before the commencement of the experiment. They were purchased from Zhejiang Weitong Lihua Laboratory Animal Co. (Zhejiang, China) and the experimental operation and procedures complied with the requirements of the Experimental Animal Ethics Committee of Wenzhou Medical University laboratory animal center. Permit No. is SYXK Zhe 2023–0034.

Pre-Prescription Studies

Equilibrium Solubility of NDNB

The equilibrium solubility of NDNB was determined using 0.1 mol/L HCl solution, pH 4.5 phosphate solution, pH 6.8 phosphate solution, water, and pH 7.4 phosphate solution as the media [10, 30]. Specifically, 10 mL of different pH media were added to 20 mL glass bottles. Excess drug material was

then added to each medium to saturation. The bottles were placed on a magnetic stirrer for 72 h at 37 ± 0.5 °C, followed by a 24-h settling period. After centrifugation at 8000 rpm, the supernatant was filtered through a 0.45 μm filter membrane. The initial filtrate was discarded, and the subsequent filtrate was collected. Three samples were prepared in parallel. Blank solutions were prepared using each respective medium. The absorbance of the diluted NDNB solutions was measured using a UV spectrophotometer (Cary300, Agilent, US) at 391 nm to calculate the solubility of NDNB in each medium (n = 3).

Oil–Water Partition Coefficient (*log P*) of NDNB

The partition coefficient (*logP*) was determined using a shaking-flask method [31, 32]. Oil phase selection includes n-octanol, whose solubility parameters are close to those of the overall biological membrane. The aqueous phase consists of water, 0.1 mol/L hydrochloric acid solution, and phosphate buffer solutions at pH 4.5, 6.8, and 7.4. The calculation of the oil–water partition coefficient involves determining the ratio of concentrations in equilibrium between n-butanol and the water phase.

Firstly, we prepared a saturated n-octanol solution in advanced. Then 15 mg of NDNB was added to 10 mL of the saturated n-octanol layer and vortexed for 5 min. After filtration with a 0.45 μm filter membrane, the absorbance of filtrate was measured using the UV and the calculated concentration was recorded as *C*.

Next, 2 mL of saturated NDNB/n-octanol solution and 2 mL of n-octanol-saturated water were mixed, vortexed for 5 min and shaken in a 37 °C water bath for 24 h, then the mixture was centrifuged at 3500 rpm for 15 min. The aqueous phase was transferred into a volumetric flask and filtered with a 0.45 μm filter membrane. The absorbance of each NDNB dilution was measured using UV at a wavelength of 391 nm. The calculated concentration was recorded as *Cw*. Further calculations for the concentration of NDNB in various media were performed. The *log P* was calculated as follows [16]:

$$log\ P\ =\ log\left(C_O/C_W\right) \tag{1}$$

$$C_O\ =\ C\ -\ C_W \tag{2}$$

Where C_O represents the concentration of NDNB in the oil phase (n-octanol), and C_W represents the concentration of NDNB in the water phase.

Preparation of the Physical Mixture (PM)

NDNB and VA64 were sieved through 80-mesh and 120-mesh screens, respectively. A binary mixture of NDNB and VA64 (drug load of 10% w/w) was prepared by mixing both in a V-shaped three-dimensional blender (VH2, Tianhe Machinery Instrument Co., Ltd, China) at 20 rpm for 15 min.

Preparation of NDNB-ASD by HME

NDNB-ASD was prepared using a co-rotating twin-screw melt extruder (ZE-16, WE-STAR Technology Suzhou Co., Ltd, China) with a diameter of 15.6 mm and a center distance of 12.5 mm at a temperature range of 80 °C-220 °C. A total of 6 zones are used, and the heating temperatures are: 80 °C, 100 °C, 140 °C, 180 °C, 200 °C, and 220 °C. The barrel is integrally formed, stainless steel fit and sealed, equipped with a building block screw, mirror polished, and the maximum torque is 16 N/m. The schematic diagram of the screw configuration is shown in Figure S2. This was facilitated by a configuration comprising a thermal standard screw with four mixing zones, and a 400 mm conveyor belt. The screw was rotated at 50 rpm, with a feeding rate ranging from 3.5 to 4.0 g/min. We selected the process parameters based on the physiochemical property investigation of the matrix material and API. VA64 has a T_g of 104 °C and starts to degrade at 230 °C. Usually, the extrusion temperature should be 30 to 50 °C above its T_g. However, the melting point of NDNB is 256 °C. We wanted to use a process temperature as high as possible to make sure the thorough dispersion and dissolution of polymers and API at a molecular level. Therefore, we selected 220 °C as the barrel temperature for the ASD preparation. As shown in Figure S3, at 220 °C, the NDNB-ASD filament appears to be transparent, uniform and light yellowish, indicating that the drug was fully melted and dispersed in the polymer homogeneously. The extrudate obtained was cooled down at room temperature (approximately 23 °C). Afterward, it was ground using a laboratory grinder, passed through 120-mesh sieves, and stored in an airtight container under ambient conditions for further use.

Characterization of NDNB-ASD

Polarized Light Microscope (PLM)

The polarized light microscopy was performed using an Olympus BX51 polarizing microscope (Ningbo Sunny Instrument Co., Ltd, China) with an objective of 20X and an ocular magnification of 10X. A small amount of sample was placed on a glass slide and handled according to standard procedures. Place the polarizer and analyzer in an orthogonal analyzing position and then examine for birefringence of the target substance [33, 34].

X-Ray Powder Diffractometry (XRPD)

XRPD was employed to investigate the physical form [35] of the NDNB-ASD made by HME along with other materials. NDNB, VA64, the PM (NDNB and VA64), and NDNB-ASD were scanned with an X-ray diffractometer (D8 Advance, Bruker Corporation, USA) with Cu-Kα radiation at 300 mA and 40 kV. The samples were placed in a micro-sample holder made of monocrystalline silicon and incorporated on a spinner stage [36], which was scanned in the 2θ range from 3° to 60° at a rate of 4°/min.

Fourier Transform Infrared Spectroscopy (FT–IR)

FT-IR (Nicolet iS50, Thermo Scientific, USA) was used to characterize the intermolecular interactions of NDNB and the carrier in solid state [37]. The analysis was done to examine interactions between the polymer with API in the physical mixture and the extrudates [38]. The bench equipment was equipped with an attenuated total reflection (ATR), arranged with a single-bounce, diamond-coated Zn-Se internal reflection element. FT-IR spectra of NDNB, VA64, the PM (NDNB and VA64) and NDNB-ASD were collected over the wave number range of 400 cm^{-1} -4000 cm^{-1} with a resolution of 4 cm^{-1}.

Differential Scanning Calorimetry (DSC)

A thermodynamic test was performed using a DSC instrument (DSC2500, TA Instruments, USA). Samples of NDNB, VA64, the PM (NDNB and VA64), and the NDNB-ASD were weighed (3–5 mg) and scanned in a nitrogen atmosphere at a heating rate of 10 °C/min from 30 °C to 300 °C. Nitrogen was provided at 30 mL/min using DSC. According to the endothermic or exothermic information reflected by the DSC curve, the change process and the existing state of NDNB in the analyzed sample can be judged [39].

Thermogravimetric Analysis (TGA)

The thermal stabilities of the NDNB-ASD and other constituents were determined by thermogravimetric analysis (TGA) [40] under nitrogen atmosphere using a Mettler Toledo TGA/DSC 1 instrument (TG209F 1 Libra, Netzsch, Germany). Samples of NDNB, VA64, the PM (NDNB and VA64), and the NDNB-ASD were weighed (1-10 mg) and performed in pin-holed aluminum crucibles at a heating rate of 10 °C/min from 30 °C to 300 °C.

Dissolution Studies of the NDNB-ASD

Analysis Methods *in Vitro* of NDNB Quantification

High-performance liquid chromatography (HPLC, Agilent1260, German) was used to quantify the drug loading of NDNB in NDNB-ASD. The chromatographic separation was performed using a C18 (250 mm, 4.6 mm ID, 5 µm) analytical column with a mobile phase consisting of a mixture of methanol and water (containing 0.05% triethylamine, pH adjusted to 4.5 with phosphate acid) at a ratio of 88:12 [9]. The flow rate was set at 1.0 mL/min, and the column temperature was maintained at 30 °C with the injection volume of 10 µL. The samples were detected at a wavelength of 391 nm. A good linear fit was observed in the range of 1–200 µg/mL, with the final calibration curve of NDNB: $A = 36.268\ C - 6.4921$ ($R^2 = 0.9999$, where A represents the area and C represents the concentration of NDNB), and the RSD (%) values of both intra-day and inter-day precision were less than 2%.

In-Vitro Dissolution of the NDNB-ASD

Dissolution studies [15, 41] of NDNB powder and NDNB-ASD were performed using a Dissolution Apparatus (RC808, Tianfa Analytical Instruments Ltd, China). The dissolution media consisted of hydrochloric acid solution with a pH of 1.0, phosphate-buffered saline (PBS) solutions with pH values of 4.5, 6.8, and 7.4, as well as distilled water. Under controlled conditions of 37 ± 1 °C and a paddle speed of 100 r/min, sink conditions were upheld. The samples (equivalent to 120 mg NDNB) were added to the dissolution medium at a volume of 900 mL. 5 mL of dissolution medium was collected at fixed time points (5, 10, 20, 30, 45, 60, 90, and 120 min), and 5 mL of fresh dissolution medium was added immediately. All samples were immediately filtered with a 0.22 µm syringe filter before quantification by HPLC. The samples were analyzed in triplicate.

Stability Studies

The stability of ASD is influenced by multiple factors and can be demonstrated through diverse methods [42]. Thermodynamics and kinetics are direct influencing factors, whereas environmental factors serve as indirect influences [43]. Among environmental factors, temperature and humidity are critical considerations. By comparing newly prepared ASD that have not undergone aging with ASD stored for a specific duration at controlled temperature and humidity conditions, observations of crystal morphology and dissolution behavior aid in assessing physical stability [44, 45]. The physical stability of the NDNB-ASD was assessed by placing the samples in stability chambers (Shanghai Yiheng

Scientific Instrument Co., Ltd, China) under conditions of temperature at 40 ± 2 °C and relative humidity at 75 ± 5%. A long-term stability study was conducted in the sealed and light-proof device for 6 months to observe for any recrystallization of NDNB-ASD [46]. XRPD analysis was conducted at each time point to monitor the potential crystallization of the solid dispersions. Additionally, selected samples underwent dissolution testing [47].

In-Vivo Pharmacokinetic Studies in Rats

Analysis Methods *in Vivo* of NDNB Quantification

According to the method described by studies [9] with some modifications, the concentration of NDNB in the plasma was investigated using a high performance liquid chromatography (HPLC, Agilent1260, Germany). The chromatographic separation was performed using a C18 (250 mm, 4.6 mm ID, 5 µm) analytical column with a mobile phase consisting of a mixture of methanol and water (containing 0.05% triethylamine, pH adjusted to 5 with phosphate acid) at a ratio of 70:30. The detection wavelength was set at 385 nm, the flow rate was maintained at 1.0 mL/min, and the column temperature maintained at 30 °C with an injection volume of 10 µL.

Pharmacokinetic Study

12 male Sprague–Dawley (SD) rats (180–220 g) were fasted for 12 h before the experiment but were allowed unrestricted access to water and then were randomly divided into four groups (n = 3). The animals were administered with the suspension (10 mL/kg) of NDNB, the PM (NDNB and VA64), NDNB-ASD, and soft capsules (Ofev®) by oral gavage. The dose of NDNB in various suspensions was 50 mg/kg. Powders such as NDNB-ASD were directly dispersed into physiological saline. For soft capsules, we utilized a syringe to extract the contents (suspension) of the capsule, followed by rinsing with physiological saline to ensure complete retrieval. Blood samples (0.2 mL blood per time point) were collected into heparinized tubes from the jugular vein pre-dose (0 h) and post-dose (0.5, 1, 1.5, 2, 3, 4, 6, 8, 10, 12, and 24 h) [16].

Plasma Sample Pretreatment

All blood samples underwent protein precipitation for processing [9, 48]. Specifically, the blood samples were centrifugated at 10000 r/min for 15 min, and the supernatant plasma was stored at − 80 °C before analysis. Each 200 µL plasma sample was mixed with 800 µL of methanol, and vortexed at 2000 rpm for 5 min, followed by centrifugation at 14000 rpm for 15 min. The supernatant was then concentrated to completely dry using a nitrogen evaporator (LC-DCY-24G, Shanghai Lichenbangxi Technology Instrument Co., Ltd, China). Subsequently, 100 µL of methanol was added for reconstitution, followed by centrifugation at 14000 rpm for 15 min. The supernatant was collected, filtered through a 0.22 µm membrane, degassed by ultrasonication, and finally transferred into sealed sample vials for HPLC analysis to calculate the NDNB concentration in the plasma.

Pharmacokinetic Data Analysis and Statistical Analysis

The calibration curve with a good linear fit spanning from 0.02 to 12 µg/mL was constructed using a weighted ($1/X^2$) least-squares linear regression of peak area ratios against concentrations. The final calibration curve of NDNB: $As/Ai = 0.7271C + 0.0568$ ($R^2 = 0.9992$, where the *As* represents the area of NDNB, the *Ai* represents the area of piperine (internal standard) and *C* represents the concentration of NDNB), and the RSD (%) values of both intra-day and inter-day precision were less than 2%. Plasma concentration–time profiles were assessed using a non-compartmental model. The important pharmacokinetic parameters, including maximum plasma concentration (C_{max}), time to reach C_{max} (T_{max}), and area under the plasma concentration–time curve ($AUC_{0-24\,h}$), were determined using Phoenix WinNonlin software (Version 8.1).

Data were collected in triplicate and presented as mean ± SD. Statistical significance was determined using a two-tailed Student's t-test, with $P < 0.05$ considered significant. Analysis of variance (ANOVA) was employed to compare results from the four groups (NDNB, physical mixture of NDNB and VA64, soft capsules (Ofev®), and NDNB-ASD) using the GraphPad Prism 10 statistical package, with significance set at $P < 0.05$.

Results and Discussion

Equilibrium Solubility and Oil–Water Partition Coefficient (*log P*) of NDNB

The key parameters influencing drug absorption are the equilibrium solubility in the gastrointestinal tract and the oil–water partition coefficient [49], as illustrated in Fig. 1. The maximum solubility of NDNB in four different media was as follows: 67.0 ± 0.7 mg/mL (pH 1.0), 88.0 ± 0.8 µg/mL (pH 4.5), 18.1 ± 1.6 µg/mL (water, pH 5.5), 12.4 ± 1.0 µg/mL (pH 6.8), and 4.1 ± 1.3 µg/mL (pH 7.4). These data indicated that NDNB exhibited higher solubility under acidic conditions, while its solubility significantly decreased under near-neutral and alkaline conditions. NDNB also contains a methyl-piperazinium group, with a reported pKa of 8.1 ± 0.1 [50] or 7.9 [51, 52]. NDNB displayed a

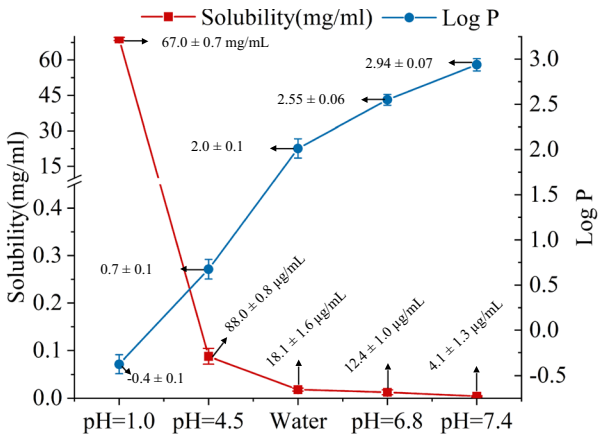

Fig. 1 Equilibrium solubility and Oil–water partition coefficient (*log P*) of NDNB in different media (mean ± SD, n = 3)

pH-dependent solubility profile with increased solubility at acidic pH < 3. At gastric pH (pH 1–2), the protonated forms (+ 1) were present, contributing to the relatively good aqueous solubility of NDNB. In a neutral or slightly acidic environment (pH 4–5.5), the degree of drug ionization was low, resulting in low solubility. In the alkaline environment of the intestine, it remained in a protonated form and exhibited extremely low solubility. In addition, its higher crystallization stability and high lattice energy may also be responsible for its lower solubility. The apparent octanol/water partition coefficient (*logP*) of NDNB in intestinal environments with pH 6.8 and 7.4 mediums was 2.55 ± 0.06 and 2.94 ± 0.07, respectively, which were close to 3. In contrast, in a pH 1.0 environment, the measurement was -0.4 ± 0.1. This suggested that NDNB was more lipophilic in the neutral and alkaline environment than in the acidic environment. The measurements are consistent with other studies that improved the dissolution of NDNB through different methods [9, 16].

Characterization of NDNB-ASD

Polarized Light Microscope (PLM)

We used a cross-polarization microscope to examine the crystalline structure [53]. As shown in Fig. 2A, when the polarizer and analyzer are oriented orthogonally, in a state known as the "crossed polar position," NDNB exhibited birefringence, showing four distinct changes in brightness during a 360° rotation, with darkness occurring every 90°. In contrast, NDNB-ASD maintained a consistently dark field of view regardless of how the specimen stage was rotated, whereas the simple physical mixture shows a mix of crystalline and amorphous regions (see Figure S4). This indicated that NDNB existed in an amorphous state.

X-ray Powder Diffractometry (XRPD)

The pure NDNB diffraction pattern in Fig. 2B exhibited characteristic intense and sharp peaks at 10.36°, 11.17°, 11.74°, 12.68°, 14.89°, 16.06°, 17.00°, 19.27°, 19.64°, and

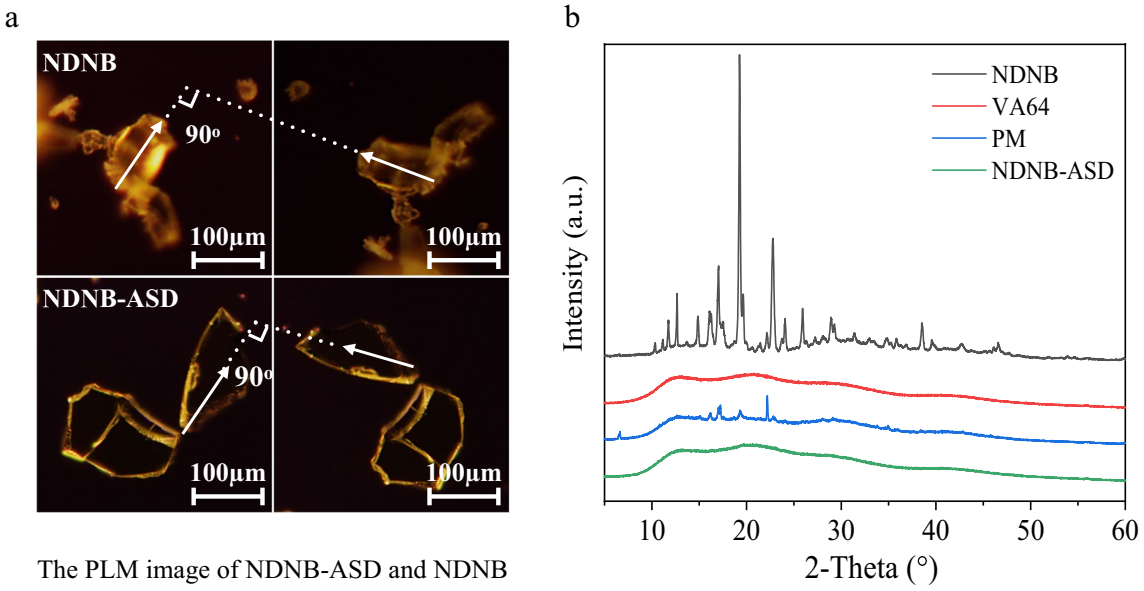

Fig. 2 **a** The polarizing microscope image of NDNB-ASD and NDNB. **b** XRPD diffractograms of NDNB, VA64, the PM (NDNB and VA64) and NDNB-ASD

22.75° at 2θ. In the physical mixture, the crystalline peaks of NDNB were weakened but not completely eradicated, indicating that NDNB remained in a crystalline state after mixing. In contrast, the X-ray diffraction pattern of the NDNB-ASD and VA64 showed no discernible peak shape; instead, the overall profile appeared broad and weak, indicating the absence of crystalline peaks. This absence of crystalline peaks indicates that NDNB was highly dispersed and stabilized in an amorphous form. Hence, this result provided ample evidence of the successful preparation of the NDNB-ASD. The successful preparation of NDNB-ASD with VA64 via HME is facilitated by the solubilization properties of VA64 [29] and the intimate mixing achieved during the extrusion process [54, 55].

Fourier Transform Infrared Spectroscopy (FT-IR)

The FT-IR spectra of NDNB, VA64, the PM (NDNB and VA64), and NDNB-ASD were depicted in Fig. 3. FT-IR spectroscopy was utilized to investigate potential molecular interactions between the drug and polymers [56, 57]. The characteristic peaks of NDNB were observed at 3550 cm^{-1}, 3450 cm^{-1} (N − H stretch), 2940 cm^{-1}, 2810 cm^{-1} (C − H stretch, CH_3), 1710 cm^{-1} (C = O stretch, ester), 1650 cm^{-1} (C = O stretch, secondary amide, 1610 cm^{-1} (C = O stretch, tertiary amide), 1520 cm^{-1}, 1440 cm^{-1}, 1290 cm^{-1} (C − N stretch), 1380 cm^{-1} (C − H in-plane bend, CH_3), 1220 cm^{-1}, 1090 cm^{-1}. VA64 has two hydrogen bond acceptor groups including its cyclic amid stretching band C = O from the lactam group (at 1660 cm^{-1}) and C = O group from the vinyl acetate ester (at 1735 cm^{-1}) [58, 59]. The PM of NDNB with VA64 exhibited both the characteristic peak of the drug and polymer. However, the spectra of ASDs showed significant changes. For the ASD formulated by VA64 and NDNB, the infrared spectrum indicated a slight shift of the C = O stretching peak of VA64 from 1735 cm^{-1} to 1731 cm^{-1}. Additionally, the C = O stretching peak of VA64 at 1660 cm^{-1} weakened and shifted to 1635 cm^{-1} [16]. The N − H stretching peak of NDNB vanished at 3450 cm^{-1}, while the C − N peak at 1520 cm^{-1} (amide II band) shifted to 1486 cm^{-1}. The above results suggested that hydrogen bond interactions may occur between the C − N bond of NDNB and the carbonyl group of VA64.

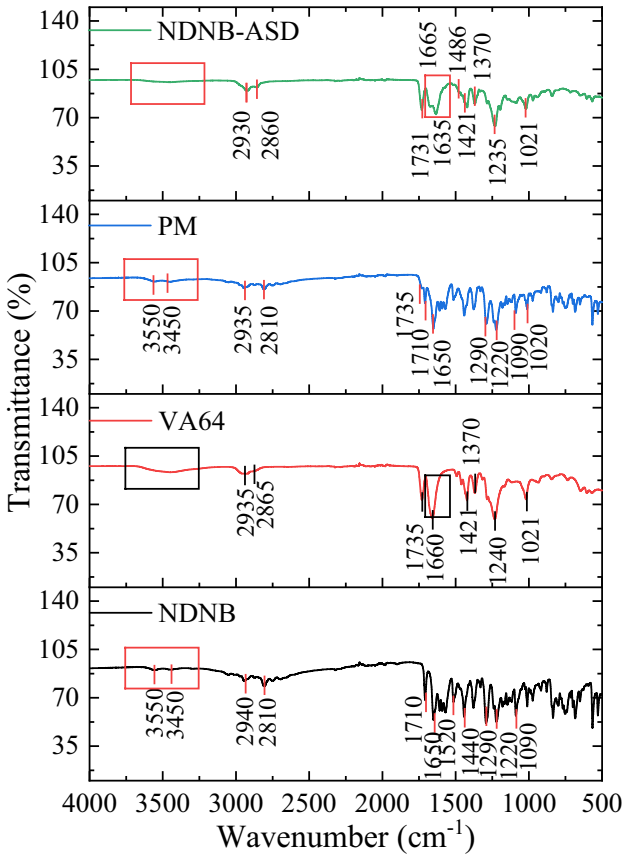

Fig. 3 ATR-FT-IR spectra of NDNB, VA64, the PM (NDNB and VA64) and NDNB-ASD

Differential Scanning Calorimetry (DSC)

As shown in Fig. 4A, the DSC curves revealed a single sharp endothermic peak at 256 °C, corresponding to melting point of NDNB. VA64 exhibited no such endothermic features, with a glass transition temperature of 107.69 °C (Fig. 4B). Absence of melting peak reveals amorphous state of polymer VA64 [60]. In the physical mixture of NDNB and VA64, the glass transition state can be observed, with midpoints recorded at 107.19 °C (Fig. 4B). The endothermic peak associated with NDNB disappeared. This can be attributed to the *in situ* drug dissolution in the polymer at a temperature higher than the polymer glass transition temperature (T_g) upon heating. In contrast, the characteristic endothermic peak of NDNB in the solid dispersion completely disappeared and the onset midpoint of the glass transition state was 104.57 °C (Fig. 4B), signifying an interaction between NDNB and VA64 during the process of preparing NDNB-ASD using HME. This interaction modified the crystalline structure of NDNB, transitioning it from a crystalline form to a stable amorphous state. However, during the first heating process of the three substances VA64, PM and NDNB-ASD, we observed that a broad endothermic peak appeared around 100 °C (Fig. 4B). This phenomenon likely indicated dehydration, coinciding precisely with the weight loss observed in TGA analysis below 100 °C (Fig. 4D). These results were consistent with solvent evaporation-induced weight loss.

Thermogravimetric Analysis (TGA)

TGA was employed to assess the weight loss attributed to the degradation of individual components in the ASD and the

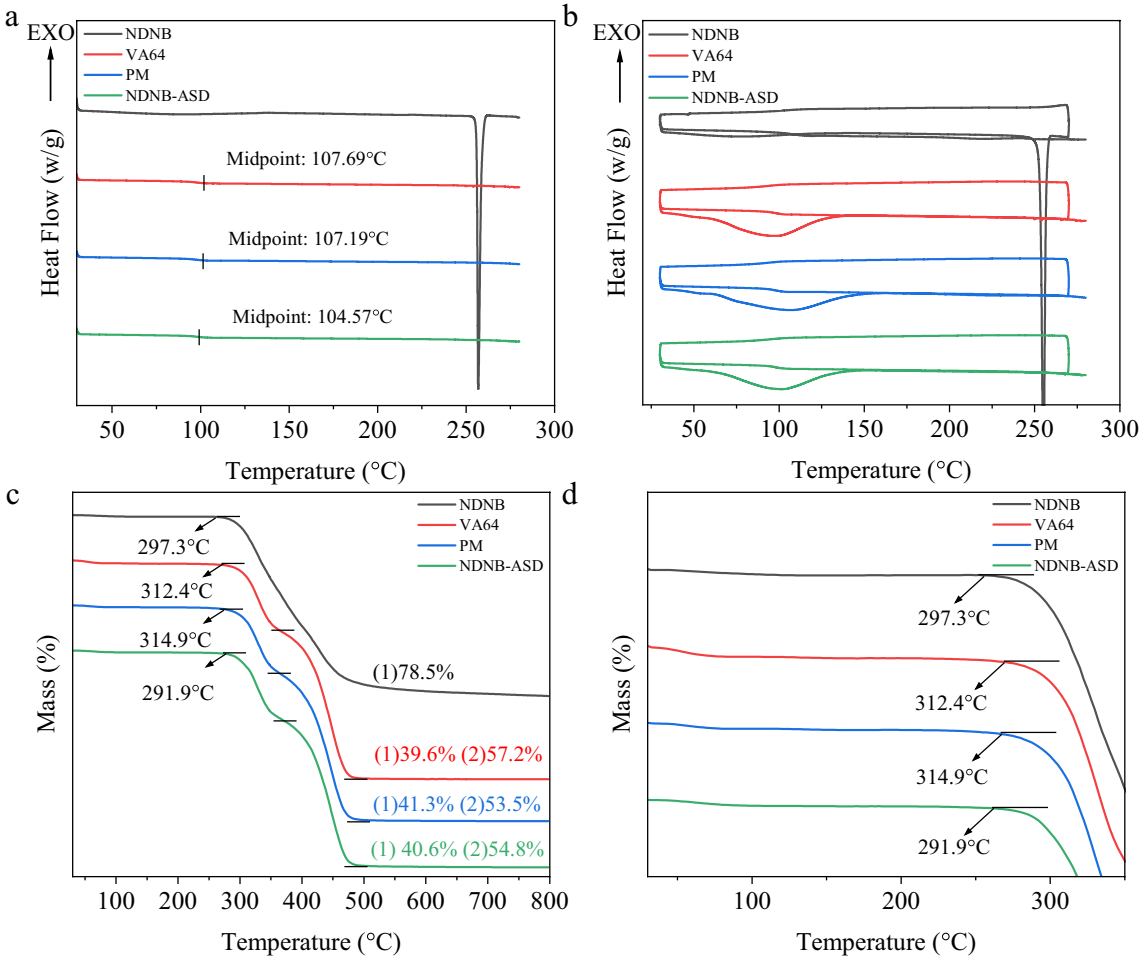

Fig. 4 **a** DSC curves of NDNB, VA64, the PM (NDNB and VA64) and NDNB-ASD in the heating range of 30–280 °C. **b** DSC curves of samples using the heat-cool-heat cycle. **c** TGA curves of NDNB, VA64, the PM (NDNB and VA64) and NDNB-ASD in the heating range of 30–800 °C. **d** TGA curves of samples in the heating range of 30–350 °C

removal of residual solvents in the processed samples [61]. The results showed that each substance had good thermal stability in the range of 30 °C to 290 °C (Fig. 4D). The initial degradation temperatures of NDNB, VA64, PM and NDNB-ASD were 297.3 °C, 312.4 °C, 314.9 °C and 291.9 °C respectively. All materials were completely degraded at around 500 °C (Fig. 4C). The TGA curves of VA64, PM, and NDNB-ASD all exhibited two distinct segments of significant weight loss, with a ratio close to 4:6. The initial segment may result from the partial degradation of vinylpyrrolidone within the VA64 molecule, while the subsequent segment may be attributed to the degradation of vinyl acetate, leading to the observed weight loss.

In-Vitro Dissolution of the NDNB-ASD

Figure 5 exhibited the profile of *in-vitro* dissolution of NDNB, PM (NDNB and VA64), and NDNB-ASD in three different buffers. In the dissolution medium at pH 1.0, the cumulative release of the three substances are essentially identical, reaching 96% within 30 min (Fig. 5A). The dissolution curves showed that the cumulative release in pH 6.8 and 7.4 phosphate buffers of NDNB-ASD was higher than that of PM, and the PM cumulative release rate was higher than that of NDNB. The cumulative release of NDNB-ASD was 8.3 times higher than that of NDNB in a pH 6.8 medium over a 2-h period (Fig. 5B) ($p < 0.0001$). In contrast, in a pH 7.4 medium, the 2-h cumulative release of NDNB-ASD was 10 times greater than that of NDNB (Fig. 5C) ($p < 0.0001$). The enhanced *in-vitro* dissolution of NDNB achieved by NDNB-ASD can be attributed to several factors. Firstly, VA64, a vinylpyrrolidone-vinyl acetate copolymer, enhances the solubility of poorly water-soluble drugs, improving wetting properties and dissolution rates [62]. Furthermore, when VA64 is immersed in the dissolving medium, the polymer surface is wetted, water penetrates into the systems and polymer surface swells to lead to the polymer chain relaxation [63]. Diffusion of drugs through

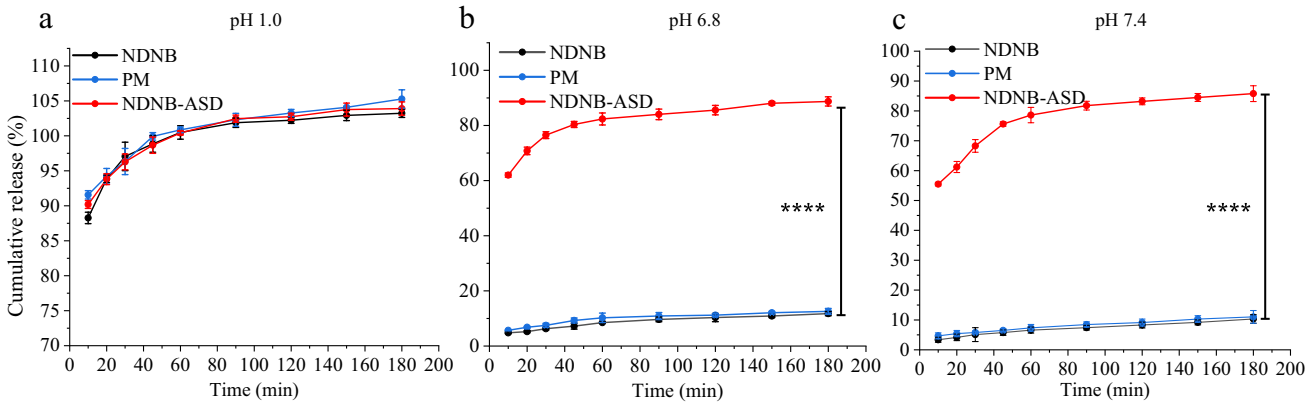

Fig. 5 Dissolution curves of NDNB, the PM (NDNB and VA64) and NDNB-ASD in different dissolution media. **a** pH 1.0 HCl. **b** pH 6.8 PBS. **c** pH 7.4 PBS

hydrated polymer networks resulting in rapid dissolution [64]. Additionally, the HME process reduces particle size and forms amorphous structures, further enhancing drug solubility and dissolution [65]. The amorphous form of NDNB in the solid dispersion contributes to its higher dissolution rate compared to its crystalline form. Homogeneous distribution within the polymer matrix by HME prevents agglomeration and promotes uniform drug release, contributing to improved release during dissolution.

Stability Studies

The physical stability of NDNB-ASD was evaluated by a stress test under 75 ± 5% humidity and 40 ± 2 °C temperature. As presented in Fig. 6, the XRPD diffraction diagrams of the NDNB-ASD after the stability test were similar to the initial systems (Fig. 6A). No diffraction peak of NDNB was detected, confirming that the drug in NDNB-ASD still existed in an amorphous state. Comparing the dissolution at 6 months with that at 0 months (Fig. 6B), The cumulative release of NDNB-ASD with different storage times intervals in the 120 min in pH of 6.8 dissolution medium can reach more than 80%. The ASD stored for 1, 3, and 6 months exhibited dissolution profiles similar to the freshly prepared (0-month) ASD. Over time, there was a slight decrease in dissolution in 180 min, with a 5.5% reduction observed in the 6-month sample compared to the 0-month sample, within the margin of error ($p > 0.05$). These results showed that NDNB-ASD remained physically stable.

In-Vivo Pharmacokinetic Studies in Rats

Pharmacokinetic parameters calculated were shown in Table I and the concentration–time curves are reported in Fig. 7. Concerning all the pharmacokinetic studies, NDNB-ASD performed best, followed by Ofev®. The bioavailability of both NDNB-ASD and Ofev® were better than NDNB and PM (NDNB and VA64). NDNB-ASD

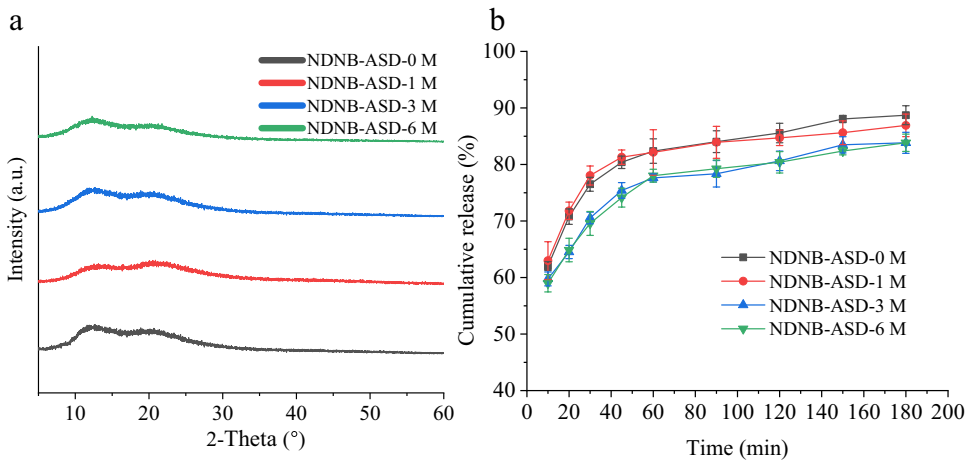

Fig. 6 **a** XRPD diffractograms of NDNB-ASD stored at different times intervals under accelerated conditions. **b** Dissolution curves of NDNB-ASD stored at different times intervals under accelerated conditions

Table I The Pharmacokinetic Parameters of NDNB, PM, NDNB-ASD and Ofev® After Being Orally Administrated in Rats at a Dose of 50 mg/kg (X ± SD, n = 3, ****$p < 0.0001$)

Parameters	NDNB	PM (NDNB + VA64)	NDNB-ASD	Ofev®
T_{max} (h)	3.0	2.0	2.0	3.0
C_{max} (μg/mL)	1.7 ± 0.2	2.05 ± 0.02	9.2 ± 0.6****	3.1 ± 0.1
$AUC_{0\text{-}24\ h}$ (μg·h/mL)	12.2 ± 1.5	15.6 3.3	64.3 ± 4.1****	27.0 ± 1.0
$AUC_{0\text{-}\infty}$ (μg·h/mL)	13.9 ± 2.7	17.0 ± 4.3	71.4 ± 4.7****	31.0 ± 1.6
Cl_F_obs (mL/h·kg)	3690.3 ± 733.1	3089.5 ± 897.9	702.2 ± 44.2	1616.5 ± 84.4
$T_{1/2}$ (h)	7.4 ± 1.7	5.7 ± 1.8	7.7 ± 2.0	8.3 ± 2.1
MRT (h)	7.2 ± 0.9	7.0 ± 1.2	7.1 ± 0.2	7.8 ± 0.3

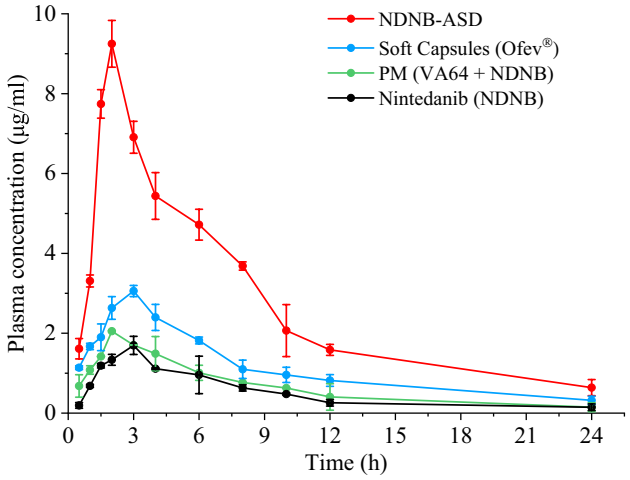

Fig. 7 *In-vivo* plasma concentration–time profiles of orally administered NDNB, the PM (NDNB and VA64), soft capsule Ofev® and NDNB-ASD in rats

demonstrated a substantial improvement in bioavailability, as evidenced by a notable increase in $AUC_{0\text{-}24\ h}$ and $AUC_{0\text{-}\infty}$ (Fig. 7). The $AUC_{0\text{-}24\ h}$ of NDNB-ASD, 64.3 ± 4.1 μg·h/mL, was 5.3 times higher than that of NDNB ($p < 0.0001$), which was 12.2 ± 1.5 μg·h/mL. And the $AUC_{0\text{-}\infty}$ of NDNB-ASD, 71.4 ± 4.7 μg·h/mL, was 5.1 times higher than that of NDNB ($p < 0.0001$), which was 13.9 ± 2.8 μg·h/mL. Additionally, the C_{max} of NDNB-ASD significantly surpassed that of NDNB, exhibiting a 5.46-fold increase in peak plasma concentration (C_{max}) (9.3 ± 0.6 μg/mL for NDNB-ASD *vs* 1.7 ± 0.2 μg/mL for NDNB) ($p < 0.0001$). This C_{max} was also higher than that of Ofev® (3.1 ± 0.1 μg/mL) and the PM (2.05 ± 0.02 μg/mL) ($p < 0.0001$). NDNB-ASD achieved its peak plasma concentration (T_{max}) at 2.0 h, whereas NDNB peaked at 3.0 h. These results demonstrate a substantial enhancement in the bioavailability of NDNB in its solid dispersion formulation.

Conclusion

By utilizing the hot melt extrusion (HME) technique, we successfully formulated NDNB amorphous solid dispersion (NDNB-ASD) characterized by an amorphous structure and remarkable stability. *In-vitro* drug release studies revealed a significantly enhanced dissolution profile for NDNB-ASD compared to NDNB alone, the physical mixture (PM), and the market product (Ofev®). Importantly, the pharmacokinetic evaluation of NDNB-ASD highlighted the efficacy of HME-prepared ASD as a potent strategy for enhancing the oral bioavailability of NDNB. This improvement is attributed to the enhanced solubility and dissolution properties, positioning NDNB-ASD as a promising formulation for optimizing therapeutic outcomes.

Supplementary Information The online version contains supplementary material available at https://doi.org/10.1208/s12249-024-02902-x.

Author Contributions Shuyin Liu and Jiantao Zhang conceptualized and designed the whole study. Shuyin Liu conducted experiments and acquired data. Jiantao Zhang and Hui Chen supervised and administrated the study. Shuyin Liu, Hui Chen, Jiantao Zhang, Feng Zhou, Sandip Tiwari, Yudong Shan and Kai Zhuang analyzed and interpreted data. Shuyin Liu and Jiantao Zhang wrote the original draft. All authors read, reviewed, edited, and approved the final manuscript.

Funding This research was supported by the Natural Science Foundation of Zhejiang Province (HDMZ23H300005).

Data Availability The data generated and/or analyzed during the current study are available from the corresponding author upon request.

Declarations

Conflicts of Interest The authors declare no conflicts of interest.

References

1. Alqahtani MS, Kazi M, Alsenaidy MA, Ahmad MZ. Advances in oral drug delivery. Front Pharmacol. 2021;12:618411. https://doi.org/10.3389/fphar.2021.618411.

2. Boyd BJ, Bergström CA, Vinarov Z, Kuentz M, Brouwers J, Augustijns P, et al. Successful oral delivery of poorly water-soluble drugs both depends on the intraluminal behavior of drugs and of appropriate advanced drug delivery systems. Eur J Pharm Sci. 2019;137:104967. https://doi.org/10.1016/j.ejps.2019.104967.
3. Li C, Wang J, Wang Y, Gao H, Wei G, Huang Y, et al. Recent progress in drug delivery. Acta Pharm Sin B. 2019;9(6):1145–62. https://doi.org/10.1016/j.apsb.2019.08.003.
4. Ghadi R, Dand N. BCS class IV drugs: Highly notorious candidates for formulation development. J Control Release. 2017;248:71–95. https://doi.org/10.1016/j.jconrel.2017.01.014.
5. Bhalani DV, Nutan B, Kumar A, Singh Chandel AK. Bioavailability enhancement techniques for poorly aqueous soluble drugs and therapeutics. Biomedicines. 2022;10(9):2055. https://doi.org/10.3390/biomedicines10092055.
6. Wang Y, Tan X, Fan X, Zhao L, Wang S, He H, et al. Current strategies for oral delivery of BCS IV drug nanocrystals: challenges, solutions and future trends. Expert Opin Drug Del. 2021;18(9):1211–28. https://doi.org/10.1080/17425247.2021.1903428.
7. Wind S, Schmid U, Freiwald M, Marzin K, Lotz R, Ebner T, et al. Clinical pharmacokinetics and pharmacodynamics of nintedanib. Clin Pharmacokinet. 2019;58:1131–47. https://doi.org/10.1007/s40262-019-00766-0.
8. Wollin L, Wex E, Pautsch A, Schnapp G, Hostettler KE, Stowasser S, et al. Mode of action of nintedanib in the treatment of idiopathic pulmonary fibrosis. Eur Respir J. 2015;45(5):1434–45. https://doi.org/10.1183/09031936.00174914.
9. Liu H, Mei J, Xu Y, Tang L, Chen D, Zhu Y, et al. Improving the oral absorption of nintedanib by a self-microemulsion drug delivery system: preparation and in vitro/in vivo evaluation. Int J Nanomed. 2019;14:8739–51. https://doi.org/10.2147/IJN.S224044.
10. Zhu Y, Fu Y, Zhang A, Wang X, Zhao Z, Zhang Y, et al. Rod-shaped nintedanib nanocrystals improved oral bioavailability through multiple intestinal absorption pathways. Eur J Pharm Sci. 2022;168:106047. https://doi.org/10.1016/j.ejps.2021.106047.
11. Liu H, Du K, Li D, Du Y, Xi J, Xu Y, et al. A high bioavailability and sustained-release nano-delivery system for nintedanib based on electrospray technology. Int J Nanomed. 2018;13:8379–93. https://doi.org/10.2147/IJN.S181002.
12. Chen C-H, Lin H-C, Wang Y-H, Wang C-Y, Lin YS, Lai C-C. The safety of nintedanib for the treatment of interstitial lung disease: A systematic review and meta-analysis of randomized controlled trials. PLoS ONE. 2021;16(5):e0251636. https://doi.org/10.1016/j.addr.2011.07.009.
13. Fukihara J, Kondoh Y. Nintedanib (OFEV) in the treatment of idiopathic pulmonary fibrosis. Expert Rev Resp Med. 2016;10(12):1247–54. https://doi.org/10.1080/17476348.2016.1249854.
14. Keating GM. Nintedanib: a review of its use in patients with idiopathic pulmonary fibrosis. Drugs. 2015;75:1131–40. https://doi.org/10.1007/s40265-015-0418-6.
15. Vaidya B, Shukla SK, Kolluru S, Huen M, Mulla N, Mehra N, et al. Nintedanib-cyclodextrin complex to improve bio-activity and intestinal permeability. Carbohyd Polym. 2019;204:68–77. https://doi.org/10.1016/j.carbpol.2018.09.080.
16. Qin Y, Xiao C, Li X, Huang J, Si L, Sun M. Enteric polymer–based amorphous solid dispersions enhance oral absorption of the weakly basic drug nintedanib via stabilization of supersaturation. Pharmaceutics. 2022;14(9):1830. https://doi.org/10.3390/pharmaceutics14091830.
17. Rimpelä A-K, Reinisalo M, Hellinen L, Grazhdankin E, Kidron H, Urtti A, et al. Implications of melanin binding in ocular drug delivery. Adv Drug Deliver Rev. 2018;126:23–43. https://doi.org/10.1016/j.addr.2017.12.008.
18. Dokania S, Joshi AK. Self-microemulsifying drug delivery system (SMEDDS)–challenges and road ahead. Drug Deliv. 2015;22(6):675–90. https://doi.org/10.3109/10717544.2014.896058.
19. Tran P, Pyo Y-C, Kim D-H, Lee S-E, Kim J-K, Park J-S. Overview of the manufacturing methods of solid dispersion technology for improving the solubility of poorly water-soluble drugs and application to anticancer drugs. Pharmaceutics. 2019;11(3):132. https://doi.org/10.3390/pharmaceutics11030132.
20. He Y, Ho C. Amorphous solid dispersions: utilization and challenges in drug discovery and development. J Pharm Sci-Us. 2015;104(10):3237–58. https://doi.org/10.1002/jps.24541.
21. Yu D-G, Li J-J, Williams GR, Zhao M. Electrospun amorphous solid dispersions of poorly water-soluble drugs: A review. J Control Release. 2018;292:91–110. https://doi.org/10.1016/j.jconrel.2018.08.016.
22. Zhang J, Guo M, Luo M, Cai T. Advances in the development of amorphous solid dispersions: The role of polymeric carriers. Asian J Pharm Sci. 2023;18(14): 100834. https://doi.org/10.1016/j.ajps.2023.100834.
23. Anane-Adjei AB, Jacobs E, Nash SC, Askin S, Soundararajan R, Kyobula M, et al. Amorphous solid dispersions: Utilization and challenges in preclinical drug development within AstraZeneca. Int J Pharmaceut. 2022;614: 121387. https://doi.org/10.1016/j.ijpharm.2021.121387.
24. Schittny A, Huwyler J, Puchkov M. Mechanisms of increased bioavailability through amorphous solid dispersions: a review. Drug Deliv. 2020;27(1):110–27. https://doi.org/10.1080/10717544.2019.1704940.
25. Pandi P, Bulusu R, Kommineni N, Khan W, Singh M. Amorphous solid dispersions: An update for preparation, characterization, mechanism on bioavailability, stability, regulatory considerations and marketed products. Int J Pharmaceut. 2020;586: 119560. https://doi.org/10.1016/j.ijpharm.2020.119560.
26. Ma X, Huang S, Lowinger MB, Liu X, Lu X, Su Y, et al. Influence of mechanical and thermal energy on nifedipine amorphous solid dispersions prepared by hot melt extrusion: Preparation and physical stability. Int J Pharmaceut. 2019;561:324–34. https://doi.org/10.1016/j.ijpharm.2019.03.014.
27. Maddineni S, Battu SK, Morott J, Majumdar S, Murthy S, Repka MA. Influence of process and formulation parameters on dissolution and stability characteristics of Kollidon® VA64 hot-melt extrudates. AAPS PharmSciTech. 2015;16(2):444–54. https://doi.org/10.1208/s12249-014-0226-4.
28. Patil H, Tiwari RV, Repka MA. Hot-melt extrusion: from theory to application in pharmaceutical formulation. AAPS PharmSciTech. 2016;17:20–42. https://doi.org/10.1208/s12249-015-0360-7.
29. Strojewski D, Krupa A. Kollidon® VA64 and Soluplus® as modern polymeric carriers for amorphous solid dispersions. Polym Med. 2022;52(1):19–29. https://doi.org/10.17219/pim/150267.
30. Ma J, Li H, Cao Z, Sha J, Sun R, He H, et al. Solid-liquid phase equilibrium of Nintedanib in ten pure solvents: Determination, thermodynamic analysis, model correlation and molecular simulation. J Chem Thermodyn. 2021;163:106595. https://doi.org/10.1016/j.jct.2021.106595.
31. Bharate SS, Kumar V, Vishwakarma AR. Determining partition coefficient (Log P), distribution coefficient (Log D) and ionization constant (pKa) in early drug discovery. Comb Chem High T Scr. 2016;19(6):461–9. https://doi.org/10.2174/1386207319666160502123917.
32. Pöstges F, Kayser K, Appelhaus J, Monschke M, Gütschow M, Steinebach C, et al. Solubility enhanced formulation approaches to overcome oral delivery obstacles of PROTACs. Pharmaceutics. 2023;15(1):156. https://doi.org/10.3390/pharmaceutics15010156.

33. Agrawal AM, Dudhedia MS, Zimny E. Hot melt extrusion: development of an amorphous solid dispersion for an insoluble drug from mini-scale to clinical scale. AAPS PharmSciTech. 2016;17:133–47. https://doi.org/10.1208/s12249-015-0425-7.
34. Davis MT, Egan DP, Kuhs M, Albadarin AB, Griffin CS, Collins JA, et al. Amorphous solid dispersions of BCS class II drugs: a rational approach to solvent and polymer selection. Chem Eng Res Des. 2016;110:192–9. https://doi.org/10.1016/j.cherd.2016.04.008.
35. Rodríguez I, Gautam R, Tinoco AD. Using X-ray diffraction techniques for biomimetic drug development, formulation, and polymorphic characterization. Biomimetics-Basel. 2020;6(1):1. https://doi.org/10.3390/biomimetics6010001.
36. Askin S, Gonçalves AD, Zhao M, Williams GR, Gaisford S, Craig DQ. A simultaneous differential scanning calorimetry–X-ray diffraction study of olanzapine crystallization from amorphous solid dispersions. Mol Pharmaceut. 2020;17(11):4364–74. https://doi.org/10.1021/acs.molpharmaceut.0c00846.
37. Chen Y, Wang S, Wang S, Liu C, Su C, Hageman M, et al. Initial drug dissolution from amorphous solid dispersions controlled by polymer dissolution and drug-polymer interaction. Pharm Res-Dordr. 2016;33:2445–58. https://doi.org/10.1007/s11095-016-1969-2.
38. Kapourani A, Valkanioti V, Kontogiannopoulos KN, Barmpalexis P. Determination of the physical state of a drug in amorphous solid dispersions using artificial neural networks and ATR-FTIR spectroscopy. Int J Pharm: X. 2020;2:100064. https://doi.org/10.1016/j.ijpx.2020.100064.
39. Dedroog S, Pas T, Vergauwen B, Huygens C, Van den Mooter G. Solid-state analysis of amorphous solid dispersions: Why DSC and XRPD may not be regarded as stand-alone techniques. J Pharmaceut Biomed. 2020;178:112937. https://doi.org/10.1016/j.jpba.2019.112937.
40. Baird JA, Taylor LS. Evaluation of amorphous solid dispersion properties using thermal analysis techniques. Adv Drug Deliver Rev. 2012;64(5):396–421. https://doi.org/10.1016/j.addr.2011.07.009.
41. Patel M, Karampuri S, Kansara V, Vyas B. Inhalable dry powder containing lipid polymer hybrid nanoparticles of Nintedanib esylate: In vitro and in vivo evaluations. J Drug Deliv Sci Tec. 2023;86:104716. https://doi.org/10.1016/j.jddst.2023.104716.
42. Lin X, Hu Y, Liu L, Su L, Li N, Yu J, et al. Physical stability of amorphous solid dispersions: a physicochemical perspective with thermodynamic, kinetic and environmental aspects. Pharm Res-Dordr. 2018;35:1–18. https://doi.org/10.1007/s11095-018-2408-3.
43. Choi J-S. RETRACTED: Enhanced stability and solubility of pH-dependent drug, telmisartan achieved by solid dispersion. J Drug Deliv Sci Tec. 2017;37:194–203. https://doi.org/10.1016/j.jddst.2017.01.001.
44. Yang Z, Nollenberger K, Albers J, Craig D, Qi S. Molecular indicators of surface and bulk instability of hot melt extruded amorphous solid dispersions. Pharm Res-Dordr. 2015;32:1210–28. https://doi.org/10.1007/s11095-014-1527-8.
45. Greco S, Authelin J-R, Leveder C, Segalini A. A practical method to predict physical stability of amorphous solid dispersions. Pharm Res-Dordr. 2012;29:2792–805. https://doi.org/10.1007/s11095-012-0717-5.
46. Lehmkemper K, Kyerematen SO, Heinzerling O, Degenhardt M, Sadowski G. Long-term physical stability of PVP-and PVPVA-amorphous solid dispersions. Mol Pharmaceut. 2017;14(1):157–71. https://doi.org/10.1021/acs.molpharmaceut.6b00763.
47. Dukeck R, Sieger P, Karmwar P. Investigation and correlation of physical stability, dissolution behaviour and interaction parameter of amorphous solid dispersions of telmisartan: a drug development perspective. Eur J Pharm Sci. 2013;49(4):723–31. https://doi.org/10.1016/j.ejps.2013.05.003.
48. Shukla SK, Kadry H, Bhatt JA, Elbatanony R, Ahsan F, Gupta V. Statistical optimization and validation of a novel ultra-performance liquid chromatography method for estimation of nintedanib in rat and human plasma. Bioanalysis. 2020;12(3):159–74. https://doi.org/10.4155/bio-2019-0284.
49. Wang X, Ren Q-W, Liu X-X, Yang Y-T, Wang B-H, Zhai R, et al. Synthesis and biological evaluation of novel H6 analogues as drug resistance reversal agents. Eur J Med Chem. 2019;161:364–77. https://doi.org/10.1016/j.ejmech.2018.10.033.
50. Dömötör O, Mathuber M, Kowol CR. In vitro biodistribution studies on clinically approved FGFR inhibitors ponatinib, nintedanib, erlotinib and the investigational inhibitor KP2692. Eur J Pharm Sci. 2024;192: 106651. https://doi.org/10.1016/j.ejps.2023.106651.
51. Dallinger C, Trommeshauser D, Marzin K, Liesener A, Kaiser R, Stopfer P. Pharmacokinetic properties of nintedanib in healthy volunteers and patients with advanced cancer. J Clin Pharmacol. 2016;56(11):1387–94. https://doi.org/10.1002/jcph.752.
52. Sieger P, Cui Y, Scheuerer S. pH-dependent solubility and permeability profiles: A useful tool for prediction of oral bioavailability. Eur J Pharm Sci. 2017;105:82–90. https://doi.org/10.1016/j.ejps.2017.04.016.
53. Tudi A, Han S, Yang Z, Pan S. Potential optical functional crystals with large birefringence: Recent advances and future prospects. Coordin Chem Rev. 2022;459: 214380. https://doi.org/10.1016/j.ccr.2021.214380.
54. Wilson M, Williams MA, Jones DS, Andrews GP. Hot-melt extrusion technology and pharmaceutical application. Ther Deliv. 2012;3(6):787–97. https://doi.org/10.4155/tde.12.26.
55. Shi Q, Moinuddin SM, Cai T. Advances in coamorphous drug delivery systems. Acta Pharm Sin B. 2019;9(1):19–35. https://doi.org/10.1016/j.apsb.2018.08.002.
56. Saerens L, Dierickx L, Quinten T, Adriaensens P, Carleer R, Vervaet C, et al. In-line NIR spectroscopy for the understanding of polymer–drug interaction during pharmaceutical hot-melt extrusion. Eur J Pharm Biopharm. 2012;81(1):230–7. https://doi.org/10.1016/j.ejpb.2012.01.001.
57. Rahma A, Munir MM, Prasetyo A, Suendo V, Rachmawati H. Intermolecular interactions and the release pattern of electrospun curcumin-polyvinyl (pyrrolidone) fiber. Biol Pharm Bull. 2016;39(2):163–73. https://doi.org/10.1248/bpb.b15-00391.
58. de Alencar Danda LJ, de Medeiros Batista L, Melo VCS, Sobrinho JLS, Soares MFDLR. Combining amorphous solid dispersions for improved kinetic solubility of posaconazole simultaneously released from soluble PVP/VA64 and an insoluble ammonio methacrylate copolymer. Eur J Pharm Sci. 2019;133:79–85. https://doi.org/10.1016/j.ejps.2019.03.012.
59. Ajay S, Harita D, Tarique M, Amin P. Solubility and dissolution rate enhancement of curcumin using kollidon® VA64 by solid dispersion technique. Int J Pharm Tech Res. 2012;4:1055–64. http://www.sphinxsai.com/2012/july_sept12/Pharm/pdfpharm/PT=23(1055-1064)%20JS%2012.pdf.
60. Ijaz QA, Latif S, Shoaib Q-U-A, Rashid M, Arshad MS, Hussain A, et al. sPreparation and characterization of ph-independent sustained-release tablets containing hot melt extruded solid dispersions of clarithromycin: tablets containing solid dispersions of clarithromycin. AAPS Pharmscitech. 2021;22:1–12. https://doi.org/10.1208/s12249-021-02115-6.

61. Budiman A, Lailasari E, Nurani NV, Yunita EN, Anastasya G, Aulia RN, et al. Ternary solid dispersions: a review of the preparation, characterization, mechanism of drug release, and physical stability. Pharmaceutics. 2023;15(8):2116. https://doi.org/10.3390/pharmaceutics15082116.
62. Wdowiak K, Pietrzak R, Tykarska E, Cielecka-Piontek J. Hot-Melt extrusion as an effective technique for obtaining an amorphous system of curcumin and piperine with improved properties essential for their better biological activities. Molecules. 2023;28(9):3848. https://doi.org/10.3390/molecules28093848.
63. Školáková T, Slámová M, Školáková A, Kadeřábková A, Patera J, Zámostný P. Investigation of dissolution mechanism and release kinetics of poorly water-soluble tadalafil from amorphous solid dispersions prepared by various methods. Pharmaceutics. 2019;11(8):383. https://doi.org/10.3390/pharmaceutics11080383.
64. Lamoudi L, Chaumeil JC, Daoud K. Swelling, erosion and drug release characteristics of Sodium Diclofenac from heterogeneous matrix tablets. J Drug Deliv Sci Tec. 2016;31:93–100. https://doi.org/10.1016/j.jddst.2015.12.005.
65. Ashour EA, Majumdar S, Alsheteli A, Alshehri S, Alsulays B, Feng X, et al. Hot melt extrusion as an approach to improve solubility, permeability and oral absorption of a psychoactive natural product, piperine. J Pharm Pharmacol. 2016;68(8):989–98. https://doi.org/10.1111/jphp.12579.